


# Wavevector-resolved polarization entanglement from radiative cascades

Received: 23 October 2024

Accepted: 20 June 2025

Published online: 05 July 2025

 Check for updates

Alessandro Laneve<sup>1,7</sup> , Michele B. Rota<sup>1,7</sup> , Francesco Basso Basset<sup>1,2,7</sup> , Mattia Beccaceci<sup>1</sup>, Valerio Villari<sup>1</sup>, Thomas Oberleitner<sup>3</sup> , Yorick Reum<sup>4</sup> , Tobias M. Krieger<sup>3</sup> , Quirin Buchinger<sup>4</sup> , Rohit Prasad<sup>4</sup> , Saimon F. Covre da Silva<sup>3,5</sup> , Andreas Pfenning<sup>4</sup> , Sandra Stroj<sup>6</sup> , Sven Höfling<sup>4</sup> , Armando Rastelli<sup>3</sup> , Tobias Huber-Loyola<sup>4</sup>  & Rinaldo Trotta<sup>1</sup>  

The generation of entangled photons from radiative cascades has enabled milestone experiments in quantum information science with several applications in photonic quantum technologies. Significant efforts are being devoted to pushing the performances of near-deterministic entangled-photon sources based on single quantum emitters often embedded in photonic cavities, so to boost the flux of photon pairs. The general postulate is that the emitter generates photons in a nearly maximally entangled state of polarization, ready for application purposes. Here, we demonstrate that this assumption is unjustified. We show that in radiative cascades there exists an interplay between photon polarization and emission wavevector, which can be further amplified by embedding the emitters in micro-cavities. We discuss how the polarization entanglement of photon pairs from a biexciton-exciton cascade in quantum dots strongly depends on their propagation wavevector and we even observe entanglement vanishing for large emission angles. Our experimental results, backed by theoretical modeling, yield a brand-new understanding of cascaded emission for various quantum emitters. In addition, our model provides quantitative guidelines for designing optical microcavities that retain both a high degree of entanglement and collection efficiency, moving the community one step further towards an ideal source of entangled photons for quantum technologies.

The employment of radiative cascades from single emitters (atoms) has been at the core of the first demonstrations of Bell inequality violation<sup>1,2</sup>. Since the outset of experimental quantum information, more “practical” solid-state emitters are being extensively exploited as quantum light sources. Radiative cascades are found in a wide variety of modern, atom-like emitters such as epitaxial<sup>3,4</sup> and colloidal<sup>5,6</sup>

quantum dots (QDs), NV-centers in diamonds<sup>7,8</sup>, molecules<sup>9,10</sup>, and defects in 2D materials<sup>11,12</sup>. In a cascaded emission, polarization entanglement of photons can directly stem from basic symmetries and selection rules<sup>13</sup>, and a two-step cascade should provide maximally polarization-entangled photon pairs; however, it is important to note that this is the case only if the pairs are collected at suitable

<sup>1</sup>Dipartimento di Fisica, Sapienza Università di Roma, Piazzale Aldo Moro 5, Roma, Italy. <sup>2</sup>Dipartimento di Fisica, Politecnico di Milano, Piazza Leonardo da Vinci 32, Milano, Italy. <sup>3</sup>Institute of Semiconductor and Solid State Physics, Johannes Kepler University, Altenbergerstraße 69, Linz, Austria. <sup>4</sup>Technische Physik, University of Würzburg, Am Hubland, Würzburg, Germany. <sup>5</sup>Universidade Estadual de Campinas, Instituto de Física Gleb Wataghin, Campinas, Brazil. <sup>6</sup>Forschungszentrum Mikrotechnik, FH Vorarlberg, Hochschulstr. 1, Dornbirn, Austria. <sup>7</sup>These authors contributed equally: Alessandro Laneve, Michele B. Rota, Francesco Basso Basset. ✉ e-mail: [alessandro.laneve@uniroma1.it](mailto:alessandro.laneve@uniroma1.it); [rinaldo.trotta@uniroma1.it](mailto:rinaldo.trotta@uniroma1.it)

wavevectors. This notion dates even back to the first demonstrations of photonic non-locality<sup>14,15</sup>, where it was predicted - but not experimentally demonstrated - that the quantum correlation between photons generated from an atomic radiative cascade depends on the light collection angle. Thus, polarization entanglement of photon pairs is intertwined with their emission pattern, which can be generally assimilated to that of two oscillating dipoles<sup>16</sup>. Nonetheless, in the successive studies and experiments that employed radiative cascades, from the oldest<sup>1,2</sup> to more recent ones<sup>3,4</sup>, this feature has been generally overlooked or neglected. The reason is straightforward: in both<sup>14</sup> and<sup>15</sup>, analytical calculations on atomic systems show that the practical consequences of this effect only become relevant for wide angles of collection. We recognize that this also holds for solid-state emitters for which, despite the presence of a preferential collection direction corresponding to the main quantization axis, the outcome of the radiative cascade for small collection angles is analogous. Emission angles away from the quantization axis, which is usually perpendicular to the sample surface, are instead hard to access due to total internal reflection<sup>17</sup>. That said, neglecting the angular dependence of the photonic state generation becomes untenable when we consider the current need to develop quantum light sources with unprecedented brightness. On-demand emitters, such as QDs, have recently been embedded in different families of cavities<sup>18–23</sup>, all with the same purpose: increasing the extraction efficiency of photons while preserving quantum correlations. In this scenario, the emitter couples with modes of the microcavity that can propagate into non-trivial optical vector fields in the far field. Thus, it is reasonable to expect that a polarization-wavevector correlation appears at yet accessible collection angles. Nevertheless, to the best of our knowledge, no experiments have ever reported on such an effect, despite the incredible efforts currently underway to optimize the performances of deterministic entangled photon sources. Here, we demonstrate experimentally the existence of a strong interplay between the degree of entanglement and light emission angle. We also developed a model for the two-photon state generated by a radiative degenerate two-level cascade that includes the angular dependence of entanglement, with which we start our discussion.

## Results

In typical radiative cascade processes here analyzed, entangled photon emission arises from the presence of a doubly-excited state, which can be written in terms of the single particle total angular momentum projection along the optical axis of collection,  $|J_{z,1}\rangle|J_{z,2}\rangle$ . In systems like QDs, where the  $z$ -axis is the main confinement direction, the doubly excited state, neglecting its dark components and fine structures, is given by<sup>24</sup>:

$$|\Psi\rangle = \frac{1}{\sqrt{2}}(|1\rangle| -1\rangle + | -1\rangle|1\rangle). \quad (1)$$

As a first step, we consider the case of an emitter in an isotropic dielectric medium. This doubly-excited state radiatively decays following the selection rule  $\Delta J = \pm 1$ , and generating a two-photon state that, given the conservation of angular momentum to the circularly polarized photons  $\{|R\rangle, |L\rangle\}$ , is maximally entangled in the polarization degree of freedom:

$$\begin{aligned} |\psi\rangle &= \frac{1}{\sqrt{2}}(|R\rangle|L\rangle + |L\rangle|R\rangle) = \\ &= \frac{1}{\sqrt{2}}(|H\rangle|H\rangle + |V\rangle|V\rangle) = |\phi^+\rangle, \end{aligned} \quad (2)$$

where  $|\phi^+\rangle$  is a maximally entangled Bell state in the linear polarization basis  $\{|H\rangle, |V\rangle\}$ . The two-photon state resulting from a degenerate radiative cascade is generally regarded as the one in Eq. (2), both for

actual atoms<sup>1,2</sup> and QDs<sup>3,4,25</sup>. However, this is true only when we consider photons propagating with  $\mathbf{k}||\mathbf{z}$ , where  $\mathbf{k}$  is the single-photon wavevector and  $\mathbf{z}$  is the confinement direction. The behavior for  $\mathbf{k} \nparallel \mathbf{z}$  is dictated by the selection rules and how they link the polarization state of a single photon generated from one transition (characterized by a given variation of total angular momentum) to its emission direction. The general  $\mathbf{k}$ -dependent state of polarization can be written in terms of polar coordinates:

$$|P_{\mathbf{k}}^\pm\rangle = N_{\mathbf{k}}(g_{\mathbf{k},\theta}^\pm|\theta\rangle + g_{\mathbf{k},\phi}^\pm|\phi\rangle), \quad (3)$$

where  $\{|\theta\rangle, |\phi\rangle\}$  represent polarization vectors along the zenithal angle  $\theta$  and the azimuthal angle  $\phi$ , the  $g_{\mathbf{k},s}^\pm$  coefficients depend on the components of the dipole moment of the  $\Delta J_z \pm 1$  transitions parallel to the  $s = \theta, \phi$  directions (see the Methods section for their expression) and  $N_{\mathbf{k}}$  is a normalization factor. We can also understand why this  $\mathbf{k}$ -dependency is needed in terms of angular momentum conservation: the projection of the total angular momentum of the excited state is transferred to the total angular momentum of the photon, which corresponds to its polarization only when it is emitted at  $\mathbf{k}||\mathbf{z}$ . For arbitrary  $\mathbf{k}$  values, the polarization only corresponds to the spin angular momentum state of the photon<sup>15</sup>.

The two transitions leading to Eq. (1) can be pictured as two radiating dipoles, which we assume as independent, and whose fields add incoherently. The intensity pattern resulting from our model in vacuum is shown in Fig. 1a for both dipole emitters, together with the total degree of polarization (DOP) as a function of the light emission angle. It is clear that as we step away from the condition  $\mathbf{k}||\mathbf{z}$ , the emission features a net DOP, due to an unbalanced mixing of the two dipole fields: at large angles, light will come mostly from one of the two dipoles, thus the emission will be endowed with the corresponding polarization. It is important to understand that the wavevector-polarization correlation that we have discussed for single photon states has also profound consequences on the degree of entanglement of photon pairs generated during the radiative decay of the state described in Eq. (1). By applying the  $\mathbf{k}$ -dependent selection rules to the total angular momentum state of Eq. (1), the polarization state changes from the case  $\mathbf{k}||\mathbf{z}$  reported in Eq. (2) to the more general expression:

$$\begin{aligned} |\psi\rangle &= A \int_{\mathbf{k},\mathbf{k}'} d\mathbf{k} d\mathbf{k}' C_{\mathbf{k}} C_{\mathbf{k}'} |\mathbf{k}, \mathbf{k}'\rangle (|P_{\mathbf{k}}^+\rangle|P_{\mathbf{k}'}^-\rangle + \\ &\quad + |P_{\mathbf{k}}^-\rangle|P_{\mathbf{k}'}^+\rangle), \end{aligned} \quad (4)$$

where  $A$  is a normalization factor,  $\mathbf{k}$  and  $\mathbf{k}'$  represent the independent modes in which the two photons can be emitted, and the  $C_{\mathbf{k}/\mathbf{k}'}$  coefficients yield the probability for a photon to be emitted in mode  $\mathbf{k}/\mathbf{k}'$ . With Eq. (4) at hand, it is instructive to visualize what the entangled two-photon state looks like for an emitter in vacuum, for which we can use a plane-wave decomposition to find an analytic form of the  $g_{\mathbf{k},s}^\pm$  coefficients as a function of  $\theta$  and  $\phi$ . For a wavevectors' pair, identified by the angles  $\{\theta, \phi, \theta', \phi'\}$ , the two-photon polarization state can be written as:

$$|\psi(\theta, \theta')\rangle = \frac{\cos(\theta) \cos(\theta') |\theta\theta'\rangle + |\phi\phi'\rangle}{\sqrt{1 + \cos(\theta)^2 \cos(\theta')^2}}. \quad (5)$$

that does not depend on  $\{\phi, \phi'\}$  because of cylindrical symmetry. If a fixed observation point is set, so that  $\theta = \theta'$ , the two-photon state becomes more and more polarized by increasing  $\theta$ , leading to a complete disruption of entanglement, as highlighted in Fig. 1b. We can intuitively understand why this is the case because at very large angles only one of the two cascade paths is collected. This introduces which-path information that reduces the degree of entanglement down to

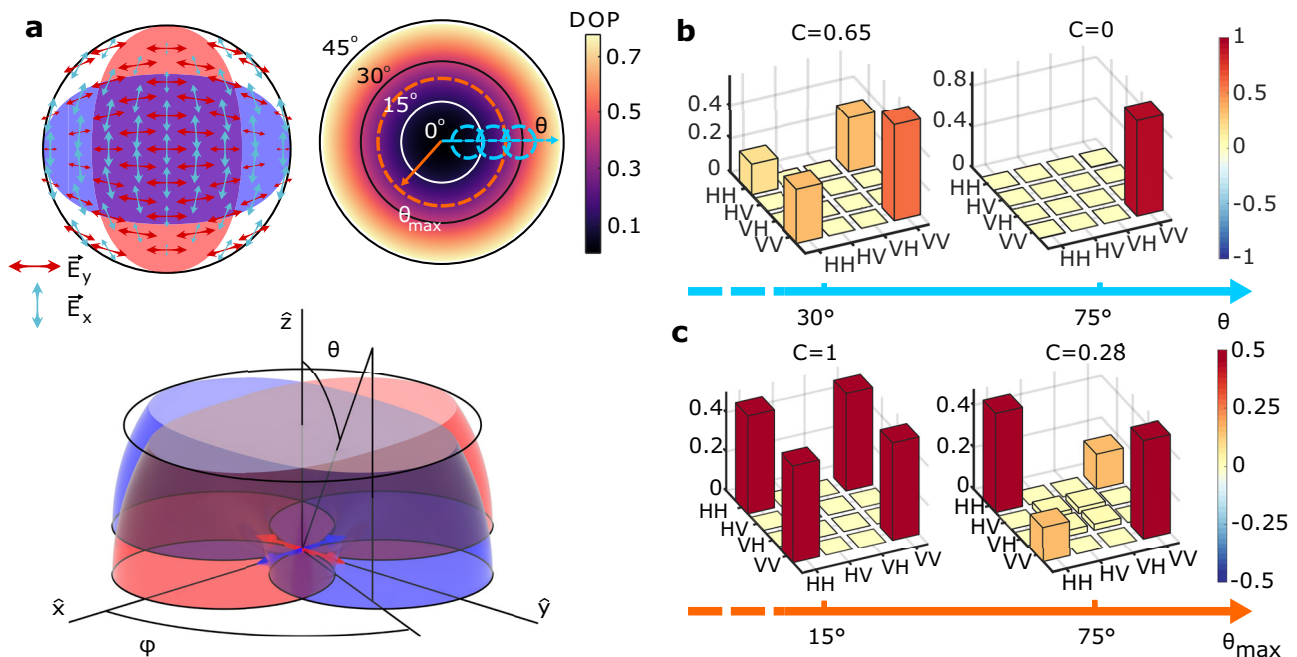


**Fig. 1 | Theoretical predictions for the polarization state of photons emitted by a radiative cascade.** **a** Bottom panel: sketch of the two emitting dipoles (blue and red arrows) with the respective isosurfaces of the radiation intensity. Top left panel: planar cut of the total emission pattern along with the direction of the electrical field oscillation for both dipole radiations, highlighting the intensity mismatch as well as the dependence of the orientation of both fields on the emission angle. Top right panel: overall degree of polarization (DOP), defined as the square root of the squared sum of the Stokes parameters (see the SI), as a function of the angles  $\phi$  and

$\theta$ . The dashed orange circle indicates a far-field region centered on the quantum emitter, corresponding to an emission angle up to  $\theta_{\max}$ . The dashed blue circles indicate different regions of  $\theta$  values that select specific wavevectors. **b** Real part of the density matrix of the two-photon entangled state for two values of  $\theta$ . The value of the concurrence for both angles is also reported. **c** Real part of the two-photon entangled state for two values of  $\theta_{\max}$ . The value of the concurrence for both angles is also reported.

zero. A more realistic light-gathering scenario is instead obtained by integrating over a solid angle of collection  $\Omega$ , which, because of cylindrical symmetry, we can describe in terms of  $\theta_{\max} = \Omega/2\pi$ , i.e., the maximum  $\theta$  for which the signal is collected. Figure 1c shows how the density matrix of the photon pair changes as we widen the collection aperture, leading again to an overall entanglement deterioration (see Supplementary Information—SI—for the analytical expression as a function of  $\theta_{\max}$  and its complete derivation). We highlight that our theory can be extended to quantum emitters with different confinement conditions by simply using the formalism we have developed and replacing the initial state in Eq. (1) as appropriate (the case of real atoms is briefly presented in the SI). To bring the above theoretical discussion into a real-life framework, we move from an emitter in a vacuum to one in a solid-state device. We chose a state-of-the-art entangled photon source: a GaAs QD in an  $\text{Al}_{0.33}\text{Ga}_{0.67}\text{As}$  membrane embedded in a circular Bragg resonator (CBR)<sup>22</sup> with a bottom broadband oxide-metal mirror. This specific structure has the advantage of a broadband collection enhancement, resulting in an overall extraction efficiency of  $\eta \approx 0.7$  for both the transitions of interest and can be integrated on top of a micromachined piezoelectric actuator to induce anisotropic strain<sup>27</sup>, as depicted in Fig. 2a. Strain engineering is used to erase the fine structure splitting between the transitions associated with the two dipoles of the emitter and generally to push the degree of entanglement close to unity when light from  $\mathbf{k} \parallel \mathbf{z}$  is collected<sup>3,27–30</sup>. Differently from the vacuum case, we cannot use a simple plane-wave expansion to find an expression for the  $|\mathbf{P}_{\mathbf{k}}^{\pm}\rangle$  vector. The two orthogonal dipoles describing a given optical transition will couple with different modes of the cavity, corresponding to different vector beams in the far field. Under this picture, Eq. (4) still holds (see the Methods section for a more formal discussion), but the coefficients  $C_{\mathbf{k}}$  and  $|\mathbf{P}_{\mathbf{k}}^{\pm}\rangle$  have to be determined by numerical simulations of the far-field emission of the emitter-cavity system. We

point out that the wavevector-polarization correlation still originates from the radiative cascade, as entanglement stems from the presence of two paths, which are described by orthogonal transition dipoles. These dipoles will now couple differently to the cavity modes and then to the photonic environment so that their far-field emission will have, in general, some degree of distinguishability that carries which-path information and degrades pure polarization entanglement. In simpler words, the effect originates from the source, while the structure around the emitter strongly dictates the specific form of the correlations (see Methods for a detailed theoretical discussion on this point). These correlations are largely connected to the vector-polarized optical field of the single-dipole cavity mode and can drastically differ from that of an emitter in vacuum.

In the domain of the CBR design, the far-field emission critically depends on the symmetry, the geometrical parameters of the cavity as well as the position of the quantum emitter, as discussed in previous works<sup>31</sup>. For this reason, we assessed the polarization-resolved emission profile of our source with dedicated experiments and simulations. To gain information on the DOP from light as a function of light emission angle (as shown in Fig. 1a for the emitter in vacuum), we assembled a Fourier microscopy setup (details in the Methods section and SI) to record the back focal plane (BFP) image of the QD emission, which contains  $\mathbf{k}$ -space information of the emitted light<sup>32</sup>. In this way, we can perform high-resolution polarimetry of the radiation far-field<sup>32–35</sup>. In Fig. 2b, c, we report the experimental intensity distribution for the single photon emission of the X to ground state transition and the corresponding DOP distribution. While more than 90% of the light is contained within  $40^\circ$ , the DOP noticeably starts deviating from zero at around  $20^\circ$  of angular aperture (the acceptance angle of an off-the-shelf multimode optical fiber) and reaches a DOP = 0.5 at around  $\theta \approx 30^\circ$ . The pattern is analogous for the XX transition, although it presents some differences that we discuss in the SI. The main features

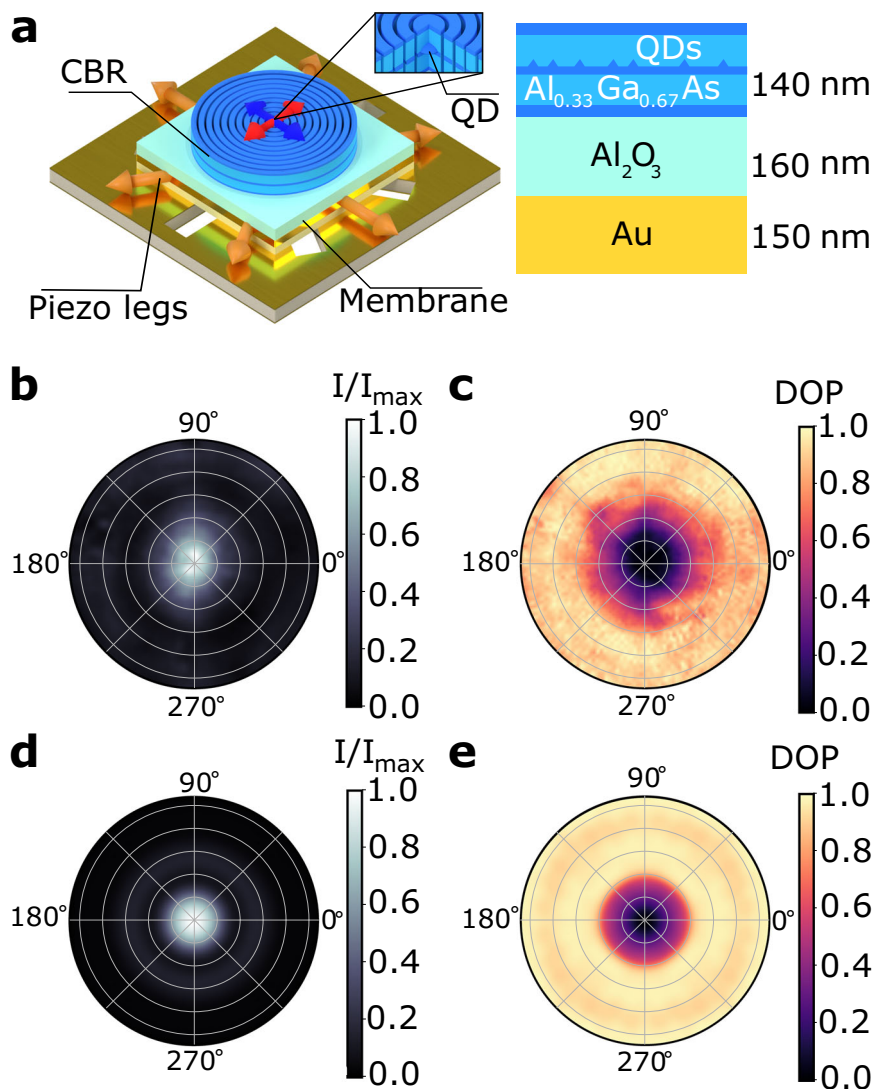


**Fig. 2 | Far-field emission and degree of polarization for quantum dots in bullseye cavities.** **a** Sketch of the CBR sample. A detailed description of the sample features is provided in the SI. **b** The experimental far-field intensity distribution for a GaAs QD in a CBR cavity and **c** corresponding DOP distribution along the radial axis. Circles represent  $10^\circ$  increments in the zenithal angle. The DOP is computed

from the Stokes parameter sampled on the far-field radiation of the QD, which was observed through BFP imaging. **d** Intensity for the CBR as computed from FDTD simulations. **e** DOP for the CBR as computed from FDTD simulations. The full Stokes parameters distributions are reported in SI.

of the experimental results are found as well in the corresponding finite-difference time-domain (FDTD) simulations of the sample emission, performed employing the Ansys Lumerical FDTD engine, both for the intensity distribution, the DOP (Fig. 2d, e, respectively), and the entire set of Stokes parameters (see the SI). Even if there is an excellent qualitative agreement between the experiments and the simulations, the latter predict a narrower cone of emission and a steeper change of DOP. These differences can be ascribed to the fact that the simulations were performed considering the nominal CBR parameters, and there is a strong dependence on the exact geometry of the micro-resonator (which cannot be easily assessed experimentally without causing damages that would alter its optical properties), as discussed in the SI. That said, the marked variations in DOP observed in Fig. 2c suggest a strong interplay between the degree of entanglement and light emission angle. To experimentally demonstrate this effect, we collect light at a specific  $k$  region, by setting up a spatial filter on the BFP image of the QD emission (see Methods). We assess the degree of entanglement of the  $k$ -selected photon pairs by

separating XX and X photons with two volume Bragg gratings and performing quantum state tomography. Multimode optical fibers are then employed to guide light to the single photon detectors used to record the coincidences needed to reconstruct the two-photon density matrices. We initially compare the density matrices sampled by scanning along the diameter of the emission cone, with a fixed narrow angular aperture, similarly to the blue circles in Fig. 1a. Figure 3a reports two examples of two-photon density matrices collected respectively at  $\theta = 20^\circ$  and  $\theta = 50^\circ$ . Alongside, in Fig. 3b, we report two main entanglement figures of merit, i.e., concurrence and fidelity, as a function of  $\theta$ . The degree of entanglement dramatically decreases when photons are collected from a highly polarized wavevector region, as highlighted by the corresponding DOP profile. Since both photons in the cascade have a defined polarization, the which-path information of the decay channel is revealed and entanglement is lost. This is also very clear inspecting the density matrix recorded for  $\theta = 50^\circ$ , showing the complete absence of the coherence terms and a fully polarized two-photon state. By exploiting FDTD simulation, we



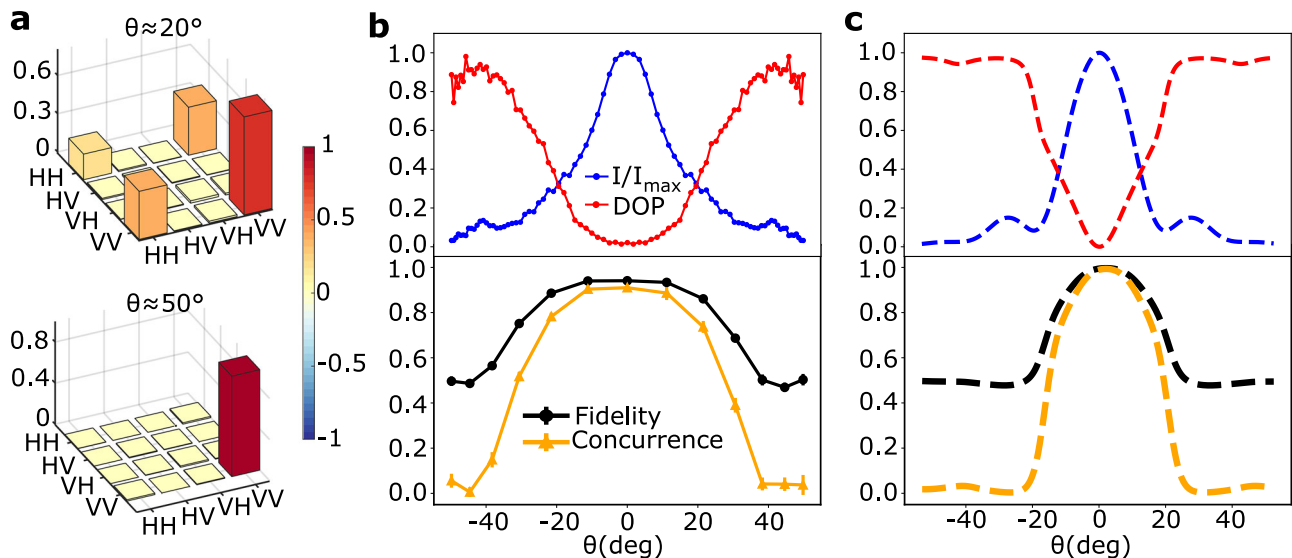


**Fig. 3 | Two-photon state and entanglement figures of merit as a function of the main collection angle for a CBR quantum dot.** **a** Two examples of experimental density matrices for different main collection angles  $\theta$ . Due to collection from a polarized wavevector region, the two-photon state has a well-defined polarization and entanglement is lost. **b** Intensity and DOP profiles as a function of  $\theta$ , extrapolated from the BFP measurements. They are reported with the corresponding fidelity of entanglement to the target state  $|\phi^+\rangle$  and concurrence, computed as a function of the main collection angle  $\theta$  and for a small  $k$  integration range (selected

by a pinhole on the BFP, see the SI). For the experimental data, we average over the azimuthal angle  $\phi$  to obtain an average profile for radiation intensity and DOP as a function of only  $\theta$ . The same quantities are reported in (c) intensity and DOP resulting from far-field FDTD simulations of the emission together with fidelity and concurrence computed on two-photon states obtained by inserting the simulated fields in Eq. (4). Error bars in the experimental data are computed assuming Poissonian distributions of coincidences and they are remarkably small due to the high number of recorded events.

are also able to predict the evolution of the entangled state for a QD in a CBR cavity. Specifically, we can compute the polarization vector of light for any wavevector and both the possible transitions, i.e., radiating dipoles. Then, we insert the normalized polarization vector in the corresponding term in Eq. (4), choosing a suitable polarization basis. Given this state, we compute quantum correlations as a function of the wavevector or range of wavevectors (for details see the SI). We report the results of this analysis in Fig. 3c, showing an excellent qualitative agreement with experimental data. Quantitatively, the main difference is related to the FDTD simulations expecting a narrower cone of emission and a steeper change of the DOP and the degree of entanglement, a discrepancy which we once again attribute to the use of the nominal CBR parameters in the simulations (see the discussion above and the SI). We performed a similar analysis also on lower extraction efficiency structures, namely GaAs QDs in planar membranes with and without DBR reflectors. As anticipated and further reported in the SI, in these cases the effect can be present but much less pronounced due to the limited access to wider and more polarized emission angles.

We performed additional experiments to investigate how the two-photon state changes as a function of the numerical aperture in the collection optics. We do that by using spatial filters with different dimensions in the BFP, similarly to the orange circle of Fig. 1a. Figure 4a highlights a rapid decrease of quantum correlation between the emitted photons as the collection half-angle  $\theta_{max}$  increases. It is important to highlight that for this type of experiment—in which we collect light with spatial filters always centered at the maximum of the light intensity profile in the BFP—the drop in the degree of entanglement is not connected to the net DOP (i.e., DOP integrated over the whole emission), which always remains below about 8%. This experimental evidence is particularly relevant to exclude that the phenomenon that we observe here could be related to possible deviations from the cylindrical symmetry of the device and/or bad positioning of the QD in the center of the cavity.

These effects would indeed result in an overall sizeable DOP<sup>36</sup>, that we instead do not observe theoretically nor experimentally (see Fig. 2). By inspecting the density matrices of Fig. 4b we can also exclude the entanglement drop we observe in Fig. 4a could be attributed to the imperfect overlap of orthogonally polarized modes<sup>37</sup>. This should result in simple decoherence<sup>37</sup> and would not justify the additional terms of state mixing that can be observed in the matrix with a larger collection aperture. More specifically, starting from Eq. (4), we can obtain the following description of the two-photon polarization density matrix:

$$\begin{aligned} \rho(\theta_{max}) = & (1 - p_1(\theta_{max}) - p_2(\theta_{max}) - p_3(\theta_{max}))|\phi^+\rangle\langle\phi^+| + \\ & + \frac{p_1(\theta_{max})}{2}(|HH\rangle\langle HH| + |VV\rangle\langle VV|) + \\ & + p_2(\theta_{max})|\psi^+\rangle\langle\psi^+| + \\ & + \frac{p_3(\theta_{max})}{2}(|HV\rangle\langle HV| + |VH\rangle\langle VH|), \end{aligned} \quad (6)$$

which contains the incoherent mixing of different terms, including  $|\psi^+\rangle = \frac{1}{\sqrt{2}}(|HV\rangle + |VH\rangle)$ , weighted by the functions  $p_1(\theta_{max})$ ,  $p_2(\theta_{max})$ , and  $p_3(\theta_{max})$  that depend on  $\theta_{max}$  and that can be numerically computed from the  $k$ -dependent polarization vectors for each dipole far-field emission. The presence of a mixing with the  $|\psi^+\rangle$  state in the experimental density matrix (see Fig. 4b for  $\theta_{max} = 54^\circ$ ) clearly rules out the imperfect overlap between two orthogonally polarized modes as the only cause of this effect. We notice that the presence of this specific mixing term is quite general and could be observed in Fig. 1c as well. Eq. (6) can be analytically calculated for the dipole-in-vacuum case and can be effectively generalized to cavity-embedded emitters under minimal symmetry assumptions, as further discussed in the SI. Finally we point out that Eq. (6) offers a valuable tool in combination with FDTD simulations to include the expected degree of entanglement in the design and optimization of a photon pair source.

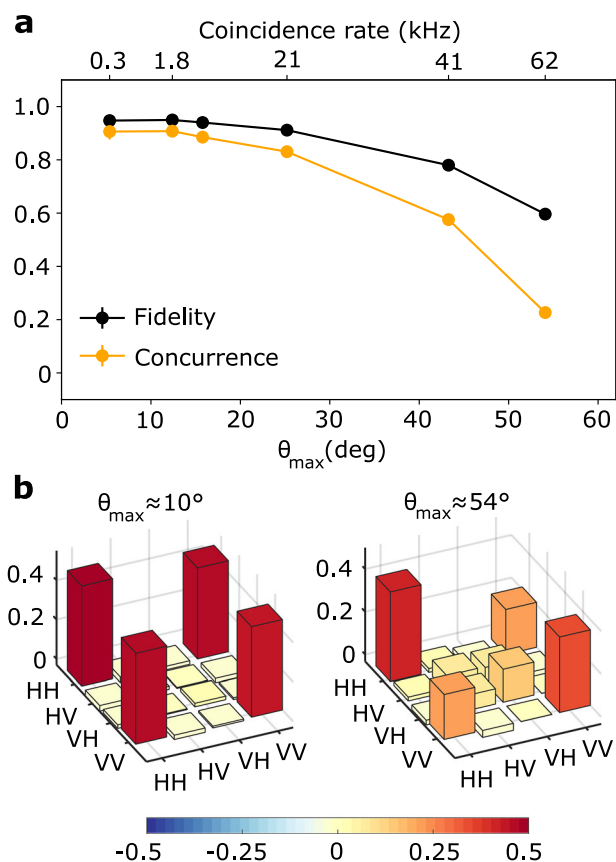


**Fig. 4 | Two-photon state and entanglement figures of merit as a function of the collection aperture for a CBR quantum dot. a** Fidelity to the  $|\phi^+\rangle$  state and concurrence as a function of different sizes of the collection region centered around the main propagation axis. Data are shown as a function of the corresponding collection half-angle  $\theta_{\max}$ . **b** Experimental density matrices corresponding to different values of  $\theta_{\max}$ , showing how the two-photon polarization state follows the description of Eq. (6). Error bars in the experimental data are computed assuming Poissonian distributions of coincidences (they are remarkably small due to the high number of recorded events).

## Discussion

Deterministic quantum emitters promise to be the next generation of quantum light sources, and their properties have been extensively studied, benchmarked and engineered. In this work, we add a previously overlooked aspect to the picture: in radiative cascades, different electronic transitions can generate radiation with distinct angular distributions. This feature produces a wavevector-polarization correlation affecting the entanglement of emitted photon pairs, a general effect that had never been witnessed. We managed to observe it for the first time in a cavity-embedded QD, due to the two paths of the radiative cascade coupling to different electromagnetic modes in the far field. We demonstrate here that the wavevector-polarization correlation is a fundamental phenomenon that arises from the basic properties of the emitter and its nanophotonic environment; this effect may pose a trade-off between the DOP-entanglement and brightness of the source in state-of-the-art photonic cavities designed to boost the flux of entangled photons. Figure 4a shows that the maximum degree of entanglement is obtained only by filtering considerably over the wavevector range in the BFP, a technique which comes at the cost of the rate of collected photon pairs. To elucidate the existence of this trade-off with quantitative data, we have eliminated the apparatus employed to scan the rear focal plane and directly coupled the QD emission into a single-mode fiber (using a set-up that

minimizes losses and is usually used in quantum communication experiments<sup>28,38</sup>) as well as in a multi-mode fiber. Whereas collecting 100% of the QD signal in multi-mode fibers delivers a 0.60(2) fidelity, the entanglement fidelity using single-mode fibers is 0.94(1) while retaining about 30% of the coincidence rate. This behavior also concurs to explain why this phenomenon has been neglected so far, as state-of-the-art quantum optics experiments are performed using single-mode fibers. That said, we strongly believe that it is possible to devise strategies that allow for preserving brightness together with the maximum degree of entanglement. One could employ the model we report here to design photonic cavities that cancel out the wavevector-polarization correlation while keeping high photon-extraction efficiency, following different possible paths, such as, for example, suitably tuning the CBR parameters. For instance, in<sup>31</sup>, as well as in our own study reported in the SI, simulations show how the mode can be tailored by small changes in the cavity parameters. We expect the wavevector-polarization effect to be milder the more the cavity mode overlaps with a Gaussian single mode in the far field, regardless of the emitter polarization. In that way, it might be possible to elude any wavevector-polarization correlation, by completely reshaping the emitter's mode through the cavity. This idea is corroborated by the simulations results we present in the SI performed on a modified CBR structure, where the effect of wavevector-polarization correlation on the degree of entanglement is much less significant. On the other hand, the discussed sensitivity to cavity and sample parameters may hinder an actual realization of a cavity with the required features; thus, fabrication accuracy must be improved too, to reach the desired results. In this sense, there have already been some interesting breakthroughs<sup>39</sup>. Another viable option would be resorting to completely alternative structures that already grant a high overlap with a single mode. Among broadband light collection strategies that are compatible with photon pairs from radiative cascades, we can cite photonic trumpets<sup>40–42</sup> and low quality factor micropillars<sup>43</sup> as approaches that have shown very good results for this metric. While having access to the polarization-resolved far-field emission of these structures would be valuable to gain further insight, single-mode fiber coupling acts as a filter on the emission mode, granting the selection of light unaffected by the polarization-sensitive mode mismatch. Thus, the search for a structure devoid of wavevector-polarization correlation can be tightly related to the quest for maximal coupling into single-mode fibers, i.e., maximally efficient photon extraction. On the other hand, it may also be possible to fully recover entanglement post-emission by polarization-sensitive manipulation of the signal wavefront, allowing for post-fabrication enhancement of various emitter-cavity systems that, however, may come at the cost of end-to-end extraction efficiency. In conclusion, our results unveil fundamental features of cascaded quantum emitters, which can impact other crucial characteristics in the development of nanophotonic systems, such as photon indistinguishability. In addition, our work points the way to engineer light-matter interaction to achieve the ultra-bright source of entangled photons required for real-life applications of quantum communication.

## Methods

### Experimental setup

The far-field images were acquired through a Fourier microscopy setup: light emitted by the QD is collected and collimated by an objective having NA = 0.81, which fixes the numerical aperture of the whole system and allows for the collection of photons emitted at a maximum angle of  $\sim 54^\circ$  to the direction orthogonal to the surface. Afterwards, a system of two lenses,  $L_1$  and  $L_2$ , suitably positioned along the photons path and featuring focal length  $f_1 = 100$  cm and  $f_2 = 40$  cm, respectively, allows to project the BFP image of the QD emission on a CCD camera sensor of  $1340 \times 100$  square pixels each of dimensions  $20 \times 20$   $\mu\text{m}$ . The different contributions due to XX-X and X-ground

transitions could be distinguished by filtering the corresponding emission lines using volume Bragg gratings<sup>44</sup> and suitable lowpass and longpass filters. To select specific  $\mathbf{k}$ -regions, an additional telescope composed of two  $f=3$  cm lenses is inserted after  $L_1$ , within its focal length. It generates another BFP image (diameter 146  $\mu\text{m}$ ) in the path towards the CCD, where by inserting a spatial filter wavevector can be selected. Thanks to removable pinholes of different sizes interposed between the two lenses in their focal points, we can select different angular ranges of wavevectors. By moving a 20  $\mu\text{m}$  diameter pinhole along the plane orthogonal to the signal propagation direction we select specific wavevectors of the radiation. The coincidence rate relative to the data reported in Fig. 2b varies from 1230 events per second for the central bin to  $\approx 1$  events per second to the outer ones. To measure the two-photon density matrix, XX and X are separately extracted using suitable volume Bragg gratings and they undergo a quantum state tomography<sup>45</sup>. Further detailed information about the setup and the source are reported in the SI.

### Theoretical model

Optical transitions are ruled by the minimal-coupling Hamiltonian<sup>16</sup>. Here, we treat single photon emission from a QD as a consequence of an exciton decay from an excited state to the ground state in a two-level system. Since we coherently pump the XX state, and the splitting between the heavy (HH) and light (LH) bands is in the order of tens of meV, a reasonable assumption is to consider only the creation of bright HH excitons. Minor changes are sufficient to also include HH-LH mixing and are left for future studies. Therefore, we will call excited and ground states respectively the conduction ( $|s\rangle|\pm\rangle$ ) and valence ( $\mp\frac{1}{\sqrt{2}}(|p_x\rangle \pm i|p_y\rangle)|\pm\rangle$ ) band states in the  $s$ -shell of the QD, where  $|s\rangle$  represents the  $s$ -type orbital, while  $|p_x\rangle$  and  $|p_y\rangle$  represent the  $p$ -orbitals, composed with the spin state  $|\pm\rangle$ . An accurate description of the output photonic state must account for the transition coupling to different possible field modes.

**Emitter in a continuous dielectric medium.** We first consider the case of a point emitter in a continuous dielectric medium. The system can be described by the Hamiltonian  $\mathcal{H} = \mathcal{H}_f + \mathcal{H}_{at} + \mathcal{H}_{int}$ , where  $\mathcal{H}_f = \sum_{\mathbf{k},s} \hbar\omega_{\mathbf{k},s} (\hat{a}_{\mathbf{k},s}^\dagger \hat{a}_{\mathbf{k},s} + \frac{1}{2})$  is the energy of the radiation field,  $\mathcal{H}_{at} = \hbar \sum_i \omega_i |i\rangle \langle i| = \hbar \sum_i \omega_i \sigma_{ii}$  is the energy of the atom-like emitter, summed over the excitonic states  $|i\rangle$ , and  $\mathcal{H}_{int}$  is the light-emitter interaction<sup>16</sup>. Assuming for simplicity the dipole approximation valid for the QD<sup>20</sup>, the interaction term  $\mathcal{H}_{int} = -\mathbf{er} \cdot \mathbf{E}$ , that regulates radiative transitions, can be written in terms of creation and annihilation operators both of photons and atomic-like excitations. Then, decomposing the electrical field in a mode basis of plane waves with given wavevector and polarization  $|\mathbf{k}, s\rangle$ ,  $\mathbf{E} = \sum_{\mathbf{k},s} A_{\mathbf{k},s} \hat{\mathbf{e}}_{\mathbf{k},s} (\hat{a}_{\mathbf{k},s} + \hat{a}_{\mathbf{k},s}^\dagger)$  where  $\hat{\mathbf{e}}_{\mathbf{k},s}$  is the polarization vector of the mode, and combining it with the dipole transition term  $\mathbf{er} = \sum_{ij} \langle i|\mathbf{er}|j\rangle |i\rangle \langle j| = \sum_{ij} \boldsymbol{\xi}_{ij} \sigma_{ij}$ , we obtain:

$$\mathcal{H}_{int} = \sum_{ij} \sum_{\mathbf{k},s} A_{\mathbf{k},s} \boldsymbol{\xi}_{ij} \cdot \hat{\mathbf{e}}_{\mathbf{k},s} \sigma_{ij} (\hat{a}_{\mathbf{k},s} + \hat{a}_{\mathbf{k},s}^\dagger) \quad (7)$$

The information about how the photon polarization is distributed in space is encoded inside the coefficients  $g_{\mathbf{k},s}^{ij} = A_{\mathbf{k},s} \boldsymbol{\xi}_{ij} \cdot \hat{\mathbf{e}}_{\mathbf{k},s} / \hbar$ . By considering a single excitation and its evolution according to  $\mathcal{H}$  via an optically allowed transition with  $\Delta J_z^\pm = \Delta J_z^\pm = \pm 1$ , after a time sufficiently longer than the radiative lifetime, the system will evolve to a product of the lower energy level of the emitter and the following photonic state<sup>16</sup>:

$$|\Psi^\pm(\mathbf{r}, t)\rangle = \sum_{\mathbf{k},s} g_{\mathbf{k},s}^\pm \frac{e^{i(\mathbf{k}\cdot\mathbf{r} - \omega_{\mathbf{k}}t)}}{\Delta_k + i\frac{\Gamma^\pm}{2}} |1\rangle_{\mathbf{k},s} = \sum_{\mathbf{k}} \frac{e^{i(\mathbf{k}\cdot\mathbf{r} - \omega_{\mathbf{k}}t)}}{\Delta_k + i\frac{\Gamma^\pm}{2}} \left( g_{\mathbf{k},\theta}^\pm |1\rangle_{\mathbf{k},\theta} + g_{\mathbf{k},\phi}^\pm |1\rangle_{\mathbf{k},\phi} \right) \quad (8)$$

being  $s = \theta, \phi$  the polar components of the polarization vector,  $\hbar\omega_{\mathbf{k}}$  the emitted photon energy (which possibly differs from the gap between upper and lower level by a quantity  $\Delta_k$ ), and  $\Gamma^\pm$  the decay rate of the excited state. From the full photonic state in Eq. (8), we can easily derive the expression of the polarization state as a function of the wavevector. In case the emitter is in vacuum, the  $A_{\mathbf{k}}$  dependence is trivial and, being  $(0, \hat{\theta}, \hat{\phi})$  a general expression for the field polarization vector  $\hat{\mathbf{e}}_{\mathbf{k}}$ , we derive a functional form of the emitted photon polarization by carrying out the scalar product between the dipole matrix element and  $\hat{\mathbf{e}}_{\mathbf{k}}$  in the oscillator strength definition.

$$|P_{\mathbf{k}}^\pm\rangle = \mp \frac{\Pi e^{\pm i\phi}}{\sqrt{2}} (\cos\theta|\hat{\theta}\rangle \pm i|\hat{\phi}\rangle) \quad (9)$$

which is what one should expect from a  $\Delta J_z = \pm 1$  transition, where we denote  $\Pi = \langle s|x|p_x\rangle = \langle s|y|p_y\rangle$ . The relative phase between  $|p_x\rangle$  and  $|p_y\rangle$  is transmitted to the photon polarization, which turns out to be circularly polarized only if we harvest light traveling along  $\hat{z}$  direction ( $\theta = 0^\circ$ ), while it becomes linearly polarized for wider zenithal collection angles. Assuming that the photon emission direction does not correlate with the transition process properties, we can build the two-photon polarization state as a composition of two coupled  $\Delta J_z = \pm 1$  cascade transitions, i.e.,

$$|\Psi_{1,2}\rangle = A \sum_{\mathbf{k}_1, \mathbf{k}_2} C_{\mathbf{k}_1} C_{\mathbf{k}_2} (|P_{\mathbf{k}_1}^+, P_{\mathbf{k}_2}^+\rangle + |P_{\mathbf{k}_1}^-, P_{\mathbf{k}_2}^+\rangle) \quad (10)$$

where  $A$  is a normalization factor, while  $C_{\mathbf{k}_1}$  and  $C_{\mathbf{k}_2}$  represent the probability amplitudes for photon 1 or 2 to be emitted along a specific direction. We can derive Eq. (4) by projecting the spatial component of the joint photonic wavefunction onto two specific  $\mathbf{k}'_1$  and  $\mathbf{k}'_2$ , i.e.,  $\langle \mathbf{k}'_1 | \langle \mathbf{k}'_2 | \Psi_{1,2} \rangle = |\Psi_{1,2}\rangle \delta(\mathbf{k}_1 - \mathbf{k}'_1) \delta(\mathbf{k}_2 - \mathbf{k}'_2)$ . We can then re-write Eq. (10) as:

$$|\Psi_{1,2}(\mathbf{k}'_1, \mathbf{k}'_2)\rangle = A C_{\mathbf{k}'_1} C_{\mathbf{k}'_2} (|P_{\mathbf{k}'_1}^+, P_{\mathbf{k}'_2}^+\rangle + |P_{\mathbf{k}'_1}^-, P_{\mathbf{k}'_2}^+\rangle) \quad (11)$$

By substituting Eq. (9) in Eq. (11), and defining the constant  $A$  from the state normalization, we can obtain the functional form of the entangled two-photon state in Eq. (5).

**Emitter in an optical microcavity.** If the emitter is placed in an optical cavity, the same result holds, but the description needs to take into account the interaction with a non-trivial photonic environment. More specifically, the transition dipoles of the QD interact with the modes of the cavity, which are coupled to radiation modes outside of the cavity. A convenient approach that extends the model used so far is to treat the output field as a reservoir coupled to the cavity modes<sup>16,46,47</sup>. The Hamiltonian of the system becomes  $\mathcal{H} = \mathcal{H}_f + \mathcal{H}_{at} + \mathcal{H}_{int} + \mathcal{H}_{res} + \mathcal{H}_{out}$  where the field operators in  $\mathcal{H}_f$  and  $\mathcal{H}_{int}$  now refer to the cavity modes rather than to plane waves. The standard design of a CBR supports only a basis of two orthogonal cavity modes that interact with the emitter and extend into the far field<sup>36</sup>. In this case,  $\mathcal{H}_f = \sum_{\pm} \hbar\omega_{\pm} (\hat{a}_{\pm}^\dagger \hat{a}_{\pm} + \frac{1}{2})$  and  $\mathcal{H}_{int} = \sum_{\pm} \hbar g_{\pm} \sigma_{\pm} (\hat{a}_{\pm} + \hat{a}_{\pm}^\dagger)$ . Moreover, there are two additional terms, one representing the energy of the photonic reservoir outside of the cavity  $\mathcal{H}_{res} = \sum_{\mathbf{k},s} \hbar\omega_{\mathbf{k},s} (\hat{b}_{\mathbf{k},s}^\dagger \hat{b}_{\mathbf{k},s} + \frac{1}{2})$  and the other describing how the cavity modes couple with this reservoir:

$$\mathcal{H}_{out} = \sum_{\pm} \sum_{\mathbf{k},s} \hbar (B_{\mathbf{k},s}^\pm \hat{a}_{\pm} \hat{b}_{\mathbf{k},s}^\dagger + B_{\mathbf{k},s}^\pm \hat{a}_{\pm}^\dagger \hat{b}_{\mathbf{k},s}) \quad (12)$$

where the terms  $\hat{b}_{\mathbf{k},s}$  are the radiation modes that are conveniently represented as a sum over plane waves with wavevector  $\mathbf{k}$  and

polarization  $s$  in the far field, while the  $B_{k,s}^{\pm}$  are coupling coefficients. To each transition dipole of the QD we can associate a vector beam in the far field. This results from an initial state of QD excitation, to its radiative decay into the cavity mode (described by  $\mathcal{H}_{int}$ ), and eventually to the coupling with the photonic modes outside the cavity (described by  $\mathcal{H}_{out}$ ). This again leads to the formula reported in Eq. (10), in which now the coefficients  $C_k$  are determined by the cavity-emitter interaction coefficients  $g^{\pm}$  and by the terms  $B_{k,s}^{\pm}$  linked to the further coupling into the external photonic reservoir<sup>46</sup>. They clearly differ from those obtained for an emitter in vacuum, where the  $C_k$  are determined solely by the coupling of the emitter to the vacuum modes. Yet, they are still connected to the probability for a photon to be emitted in a specific direction and can be obtained, together with the polarization field, from the numerical solution of Maxwell's equations via FDTD simulations of each emission dipole inside the optical microcavity. Empiric information on these quantities can be obtained using polarization-resolved Fourier microscopy, as discussed in the main text.

## Data availability

The data supporting the results of this paper are available in the main text and the Supplementary Information. Further data are available from the corresponding authors upon request.

## Code availability

The code supporting the analysis reported in this paper is available from the corresponding authors upon reasonable request.

## References

- Freedman, S. J. & Clauser, J. F. Experimental test of local hidden-variable theories. *Phys. Rev. Lett.* **28**, 938 (1972).
- Aspect, A., Grangier, P. & Roger, G. Experimental tests of realistic local theories via Bell's theorem. *Phys. Rev. Lett.* **47**, 460 (1981).
- Benson, O., Santori, C., Pelton, M. & Yamamoto, Y. Regulated and entangled photons from a single quantum dot. *Phys. Rev. Lett.* **84**, 2513 (2000).
- Akopian, N. et al. Entangled photon pairs from semiconductor quantum dots. *Phys. Rev. Lett.* **96**, 130501 (2006).
- Yin, C. et al. Bright-exciton fine-structure splittings in single perovskite nanocrystals. *Phys. Rev. Lett.* **119**, 026401 (2017).
- Utzat, H. et al. Coherent single-photon emission from colloidal lead halide perovskite quantum dots. *Science* **363**, 1068–1072 (2019).
- Togan, E. et al. Quantum entanglement between an optical photon and a solid-state spin qubit. *Nature* **466**, 730–734 (2010).
- Ruf, M., Wan, N. H., Choi, H., Englund, D. & Hanson, R. Quantum networks based on color centers in diamond. *J. Appl. Phys.* **130**, 070901 (2021).
- Nordén, B. Entangled photons from single atoms and molecules. *Chem. Phys.* **507**, 28–33 (2018).
- Rezai, M., Wrachtrup, J. & Gerhardt, I. Polarization-entangled photon pairs from a single molecule. *Optica* **6**, 34–40 (2019).
- He, Y.-M. et al. Cascaded emission of single photons from the biexciton in monolayered WS<sub>2</sub>. *Nat. Commun.* **7**, 13409 (2016).
- Tonndorf, P. et al. Single-photon emitters in gas. *2D Mater.* **4**, 021010 (2017).
- Yang, C. N. Selection rules for the dematerialization of a particle into two photons. *Phys. Rev.* **77**, 242 (1950).
- Clauser, J. F., Horne, M. A., Shimony, A. & Holt, R. A. Proposed experiment to test local hidden-variable theories. *Phys. Rev. Lett.* **23**, 880 (1969).
- Shimony, A. Foundations of quantum mechanics. *Proc. Intern. Sch. Phys. Enrico Fermi* **182**, 1082–1090 (1971).
- Scully, M. O. & Zubairy, M. S. *Quantum Optics*. (Cambridge University Press, 1997).
- Benisty, H., Stanley, R. & Mayer, M. Method of source terms for dipole emission modification in modes of arbitrary planar structures. *JOSA A* **15**, 1192–1201 (1998).
- Gérard, J.-M. et al. Enhanced spontaneous emission by quantum boxes in a monolithic optical microcavity. *Phys. Rev. Lett.* **81**, 1110 (1998).
- Hennessy, K. et al. Quantum nature of a strongly coupled single quantum dot–cavity system. *Nature* **445**, 896–899 (2007).
- Lodahl, P., Mahmoodian, S. & Stobbe, S. Interfacing single photons and single quantum dots with photonic nanostructures. *Rev. Mod. Phys.* **87**, 347 (2015).
- Dousse, A. et al. Ultrabright source of entangled photon pairs. *Nature* **466**, 217–220 (2010).
- Liu, J. et al. A solid-state source of strongly entangled photon pairs with high brightness and indistinguishability. *Nat. Nanotechnol.* **14**, 586–593 (2019).
- Wang, H. et al. On-demand semiconductor source of entangled photons which simultaneously has high fidelity, efficiency, and indistinguishability. *Phys. Rev. Lett.* **122**, 113602 (2019).
- Juska, G. et al. Conditions for entangled photon emission from (111) b site-controlled pyramidal quantum dots. *J. Appl. Phys.* **117**, 134302 (2015).
- Hudson, A. et al. Coherence of an entangled exciton-photon state. *Phys. Rev. Lett.* **99**, 266802 (2007).
- Huo, Y., Rastelli, A. & Schmidt, O. Ultra-small excitonic fine structure splitting in highly symmetric quantum dots on GaAs (001) substrate. *Appl. Phys. Lett.* **102**, 152105 (2013).
- Rota, M. B. et al. A source of entangled photons based on a cavity-enhanced and strain-tuned GaAs quantum dot. *eLight* **4**, 1–13 (2024).
- Basso Basset, F. et al. Quantum key distribution with entangled photons generated on demand by a quantum dot. *Sci. Adv.* **7**, eabe6379 (2021).
- Trotta, R. et al. Wavelength-tunable sources of entangled photons interfaced with atomic vapours. *Nat. Commun.* **7**, 10375 (2016).
- Huber, D. et al. Highly indistinguishable and strongly entangled photons from symmetric GaAs quantum dots. *Nat. Commun.* **8**, 15506 (2017).
- Rickert, L., Kupko, T., Rodt, S., Reitzenstein, S. & Heindel, T. Optimized designs for telecom-wavelength quantum light sources based on hybrid circular Bragg gratings. *Opt. Exp.* **27**, 36824–36837 (2019).
- Lieb, M. A., Zavislan, J. M. & Novotny, L. Single-molecule orientations determined by direct emission pattern imaging. *JOSA B* **21**, 1210–1215 (2004).
- Osorio, C. I., Mohtashami, A. & Koenderink, A. F. K-space polarimetry of bullseye plasmon antennas. *Sci. Rep.* **5**, 9966 (2015).
- Li, L. et al. Efficient photon collection from a nitrogen vacancy center in a circular bullseye grating. *Nano Lett.* **15**, 1493–1497 (2015).
- Fons, R. et al. All-optical mapping of the position of quantum dots embedded in a nanowire antenna. *Nano Lett.* **18**, 6434–6440 (2018).
- Peniakov, G. et al. Polarized and unpolarized emission from a single emitter in a bullseye resonator. *Laser Photon. Rev.* **18**, 2300835 (2024).
- Larqué, M., Karle, T., Robert-Philip, I. & Beveratos, A. Optimizing h1 cavities for the generation of entangled photon pairs. *N. J. Phys.* **11**, 033022 (2009).
- Rota, M. B., Basset, F. B., Tedeschi, D. & Trotta, R. Entanglement teleportation with photons from quantum dots: toward a solid-state based quantum network. *IEEE J. Sel. Top. Quant. Electron.* **26**, 1–16 (2020).
- Rickert, L. et al. High purcell enhancement in quantum-dot hybrid circular Bragg grating cavities for GHz clock rate generation of indistinguishable photons. *ACS Photon.* **12**, 464–475 (2024).



40. Claudon, J. et al. A highly efficient single-photon source based on a quantum dot in a photonic nanowire. *Nat. Photon.* **4**, 174–177 (2010).
41. Munsch, M. et al. Dielectric gas antenna ensuring an efficient broadband coupling between an InAs quantum dot and a Gaussian optical beam. *Phys. Rev. Lett.* **110**, 177402 (2013).
42. Stepanov, P. et al. Highly directive and Gaussian far-field emission from “giant” photonic trumpets. *Appl. Phys. Lett.* **107**, 141106 (2015).
43. Ginés, L. et al. High extraction efficiency source of photon pairs based on a quantum dot embedded in a broadband micropillar cavity. *Phys. Rev. Lett.* **129**, 033601 (2022).
44. Glebov, A. L. et al. Volume Bragg gratings as ultra-narrow and multiband optical filters. *Micro-Opt.* **8428**, 42–52 (2012).
45. James, D. F., Kwiat, P. G., Munro, W. J. & White, A. G. Measurement of qubits. *Phys. Rev. A* **64**, 052312 (2001).
46. Cui, G. & Raymer, M. Emission spectra and quantum efficiency of single-photon sources in the cavity-qed strong-coupling regime. *Phys. Rev. A* **73**, 053807 (2006).
47. Naesby, A., Suhr, T., Kristensen, P. T. & Mørk, J. Influence of pure dephasing on emission spectra from single photon sources. *Phys. Rev. A-At. Mol. Opt. Phys.* **78**, 045802 (2008).

## Acknowledgements

This project has received funding from the European Union’s Horizon 2020 research and innovation program under Grant Agreement no. 899814 (Europe) and No. 871130 (Ascent+), and from the QuantERA II program that has received funding from the European Union’s Horizon 2020 research and innovation program under Grant Agreement No 101017733 via the project QD-E-QKD and the FFG grant no. 891366. The authors also acknowledge support from MUR (Ministero dell’Università e della Ricerca) through the PNRR MUR project PEO00023-NQSTI, the European Union’s Horizon Europe research and innovation program under EPIQUE Project GA No. 101135288, the Austrian Science Fund (FWF) via the Research Group FG5, I 4320, I 4380, and the Linz Institute of Technology (LIT), the LIT Secure and Correct Systems Lab, supported by the State of Upper Austria. T.H.L. acknowledges financial support from the German Ministry of Education and Research (BMBF) within the Project Qecs (Förderkennzeichen 13N16272). S.F.C da Silva thanks FAPESP for financial support under the projects 2024/08527-2 and 2024/21615-8. We thank Paolo Mataloni and Emanuele Pelucchi for useful discussion.

## Author contributions

A.L., M.B.R., and F.B.B. contributed equally to the results of the paper. A.L., M.B., and F.B.B. developed the theoretical model for the polarization state of photon pairs, as well as the corresponding numerical simulations. A.L., M.B.R., M.B., V.V., and F.B.B. performed the experiment with help from R.T. M.B.R., M.B., V.V., and F.B.B. designed the

experimental setup. F.B.B. and R.T. designed the source setup. T.O., Y.R., Q.B., R.P., and T.H.L. provided numerical simulations data to support experimental results with the supervision of A. P. and T.H.L. S.F.C.d.S., and A.R. designed and grew the QD sample. M.B.R., T.M.K, Q.B., and S.S., designed and processed the cavity of the QD with the supervision of R.T., A.R., T.H.L., and S.H.A.L. wrote the manuscript, with feedback from all the authors. The project was conceived and coordinated by R.T.

## Competing interests

The authors declare no competing interests.

## Additional information

**Supplementary information** The online version contains supplementary material available at <https://doi.org/10.1038/s41467-025-61460-3>.

**Correspondence** and requests for materials should be addressed to Alessandro Laneve or Rinaldo Trotta.

**Peer review information** *Nature Communications* thanks the anonymous reviewers for their contribution to the peer review of this work. A peer review file is available.

**Reprints and permissions information** is available at <http://www.nature.com/reprints>

**Publisher’s note** Springer Nature remains neutral with regard to jurisdictional claims in published maps and institutional affiliations.

**Open Access** This article is licensed under a Creative Commons Attribution-NonCommercial-NoDerivatives 4.0 International License, which permits any non-commercial use, sharing, distribution and reproduction in any medium or format, as long as you give appropriate credit to the original author(s) and the source, provide a link to the Creative Commons licence, and indicate if you modified the licensed material. You do not have permission under this licence to share adapted material derived from this article or parts of it. The images or other third party material in this article are included in the article’s Creative Commons licence, unless indicated otherwise in a credit line to the material. If material is not included in the article’s Creative Commons licence and your intended use is not permitted by statutory regulation or exceeds the permitted use, you will need to obtain permission directly from the copyright holder. To view a copy of this licence, visit <http://creativecommons.org/licenses/by-nc-nd/4.0/>.

© The Author(s) 2025